Supporting Information

Huang et al. 10.1073/pnas.1116862109

SI Materials and Methods

Preparation of Reaction Center Crystals. "Wild-type," polyhistidine-tagged reaction centers (RCs) were obtained from a strain of *Rb. sphaeroides* that lacked the light-harvesting II complex. Cells were grown chemoheterotrophically (semiaerobic, dark, 34 °C). RCs were extracted from the cell membranes using the detergent lauryldimethylamine N-oxide (LDAO) and purified using Ni-NTA (nitrilotriacetic acid) immobilized metal affinity chromatography as previously described (1, 2). The detergent LDAO was replaced for octyl β-D-glucopyranoside (OG) by applying the RCs to an anionic exchange column, and eluting the RC in a buffer containing 0.8% (wt/vol) OG, 280 mM NaCl, 10 mM Tris, 1 mM EDTA and pH 7.8. Crystallization in the needle-shaped orthorhombic ($P2_12_12_1$) space group was accomplished by vapor diffusion in the presence of polyethy1ene glycol (PEG) 4000 using methods described earlier (3–5).

Calculation of Cofactor Optical Absorption Transitions Along Crystal Axes. Projections for the cofactor optical transition dipole moments onto the orthorhombic crystal $P2_12_12_1$ unit cell ***a***, ***b***, and ***c*** axes were calculated using coordinates from the Protein Data Bank entry 4RCR (6). The bacteriochlorophyll and bacteriopheophytin Q_y and Q_x directions were taken as lying along the pyrrole ring I to III and the pyrrole ring II to IV nitrogen-to-nitrogen directions, respectively (7). Optical absorption contributed by the transition dipole moment for each cofactor, $A(\lambda) = (\vec{E} \bullet \vec{m})^2 \varepsilon \cdot f(\lambda)$, is the dot product for the unit vectors for the light electric field, $\vec{E}$, and the cofactor transition dipole moment, $\vec{m}$, weighted by the extinction coefficient, ε, and lineshape function, $f(\lambda)$. When the light field is aligned along the orthogonal axes of the crystal unit cell, ***a***, ***b***, ***c***, the absorption can be expressed as the extinction coefficient weighted transition dipole projections: $A_{a,b,c}(\lambda) = \cos^2 \vartheta_{a,b,c} \varepsilon \cdot f(\lambda)$. The reaction center $P2_12_12_1$ unit cell was reconstructed from the crystal coordinates using the program Mercury provided by the Cambridge Crystallographic Database Center (http://www.ccdc.cam.ac.uk/products/mercury/).

The Q_x and Q_y transition dipole projections, $\cos^2 \vartheta_{a,b,c}$, were calculated for each cofactor in the four reaction center complexes that comprise the unit cell. The calculation confirmed that for the $P2_12_12_1$ symmetry group, each of the four reaction centers in the unit cell makes an equivalent contribution along the unit cell directions. The calculated cofactor transition dipole moment projections were weighted according to their corresponding extinction coefficients (8) to provide an crystal coordinate-based index of predicted optical absorption along the unit cell principle axes directions. The resulting weighted amplitudes for the BChl and BPh Q_x and Q_y transition moments projected using the crystallographic axes ***a***, ***b***, and ***c*** defined in the 4RCR Protein Data Bank entry (6).

We note that the definition for the crystallographic axes for the *Rb. sphaeroides* $P2_12_12_1$ crystals differs for the UC San Diego 4RCR (6) and Argonne 2RCR (3–5) structures, but the unit cell packing is equivalent. The 4RCR crystallographic ***a***, ***b***, ***c*** axes correspond to the 2RCR ***b***, ***c***, ***a*** axes respectively. Our previous X-ray alignment measurements showed that the unit cell directions lie parallel to the crystal axes, with 2RCR ***a*** axis (4RCR ***c*** axis) aligned along the crystal long axis (4, 5). This conclusion is supported the low temperature optical dichroism analysis presented in Fig. 1 and our earlier room temperature optical dichroism measurements (9), and by triplet state EPR (10) and preliminary assessment of carotenoid optical dichroism (11) in *Rb. sphaeroides* $P2_12_12_1$ crystals. In Fig. 1 and our earlier publication (9) we used the 4RCR crystallographic axes definition.

Sample Preparation for Low Temperature Optical Measurements. Cryogenic temperature of approximately 100 k was achieved by flowing cold nitrogen stream through a home-built vacuum-sealed rectangular glass housing. For detergent-solubilized RCs in solution, 60% (vol/vol) ethylene glycol was employed as a cryoprotectant. For crystals, a cryoprotectant consisting of 1.5 M sucrose was employed with 25% (wt/vol) PEG 400, 0.5 M NaCl, and 20 mM Tris pH 7.8 added to form optical clear glass at 100 K and to preserve the structure and photochemical function of RC crystals. 50 mM of dithionite was added immediately prior to the freezing to reduce the primary donor (special pair bacteriochlorophyll dimer) P. The RC solution with ethylene glycol or RC crystals of interest were drawn into a capillary with 0.2 mm × 2 mm cross-sections (VitroCom) with the cryoprotectant through capillary action and the capillary was consequently sealed with beeswax. The sealed capillary was placed inside the rectangular glass housing that is position on a X-Y-Z translational stage.

Ground State Absorption Spectroscopy of Cryogenically Cooled RC Crystals. Polarized ground state absorption spectra were acquired by a home-built microscope equipped with an optical spectrograph (Princeton Instrument) and a thermoelectric cooled CCD (Princeton Instrument). A 10X, 0.25 numerical aperture microscope objective was used to focus a halogen white light source to a spot size of approximately 5 μm. A broadband linear polarizer was placed immediately after the light source to control the polarization. Transmitted light was collected by a long working distance 10x 0.28 NA objective (30 mm working distance, Mitutoyo) and subsequently detected by the spectrograph and CCD combination.

Low Temperature (100K) Transient Absorption Spectroscopy. The experiments were performed with a Spectra Physics amplified Ti:Sapphire laser system that coupled to an TOPAS optical parametric amplifier. The TOPAS provided 130 fs pump pulses that were tunable from 450 nm-2,000 nm at 1.7 KHz. The probe pulse was a coherent white light continuum generated by focusing a small fraction (<1%) of the Ti: Sapphire amplifier output at 800 nm onto a 3 mm thick sapphire window. An Ultrafast System femtosecond transient absorption spectrometer was employed for the data acquisition. In order to avoid damage to the crystals, the laser pump power was maintained at less than 50 nJ/pulse with light focused to a spot size of approximately 20 μm. Transmission of the probe was collected by a long working distance 10x 0.28 NA objective (30 mm working distance, Mitutoyo) and a video camera was employed to view crystal. The polarizations of the pump and probe beams were controlled independently by two ½ waveplates.

1. Fritzsch G (1998) Obtaining crystal structures from bacterial photosynthetic reaction centers. *Photosynthesis: Molecular Biology of Energy Capture* 297:57–77.
2. Goldsmith JO, Boxer SG (1996) Rapid isolation of bacterial photosynthetic reaction centers with an engineered poly-histidine tag. *Biochimica Et Biophysica Acta-Bioenergetics* 1276:171–175.
3. Chang C-H, El-Kabbani O, Tiede DM, Norris J, Schiffer M (1991) Structure of the membrane-bound protein photosynthetic reaction center from *Rhodobacter sphaeroides*. *Biochemistry* 30:5352–5360.
4. Chang C-H, Schiffer M, Tiede DM, Smith U, Norris JR (1985) Characterization of bacterial photosynthetic reaction center crystals from *Rhodopseudomonas sphaeroides* R-26 by X-ray diffraction. *J Mol Biol* 186:201–203.
5. Chang C-H, Tiede D, Tang D, Smith U, Norris J, Schiffer M (1986) Structure of *Rhodopseudomonas sphaeroides* R-26 reaction center. *FEBS Letts* 205:82–86.
6. Yeates TO, et al. (1988) Structure of the reaction center from Rhodobacter sphaeroides R-26 and 2.4.1: protein-cofactor (bacteriochlorophyll, bacteriophytin, and carotenoid) interactions. *Proc Natl Acad Sci USA* 85:7993–7997.
7. Parson WW, Warshel A (1987) Spectroscopic properties of photosynthetic reaction centers. 2. Application of the theory to *Rhodopseudomonas viridis*. *J Am Chem Soc* 109:6152–6163.
8. Straley SC, Parson WW, Mauzerall DC, Clayton RK (1973) Pigment content and molar extinction coefficients of photochemical reaction centers from Rhodopseudomonas spheroides. *Biochim Biophys Acta* 305:597–609.
9. Huang L, et al. (2008) Correlating ultrafast function with structure in single crystals of the photosynthetic reaction center. *Biochemistry* 47:11387–11389.
10. Gast P, Norris JR (1984) EPR detected triplet fromation in a single crystal of reaction center protein from the photosynthetic bacterium *Rhodopseudomonas sphaeroides* R-26. *FEBS Letts* 177:277–280.
11. Frank HA, Taremi SS, Knox JR (1987) Crystallization and preliminary X-ray and optical spectroscopic characterization of the photochemical reaction center from *Rhodobacter sphaeroides* strain 2.4.1. *J Mol Biol* 198:139–141.

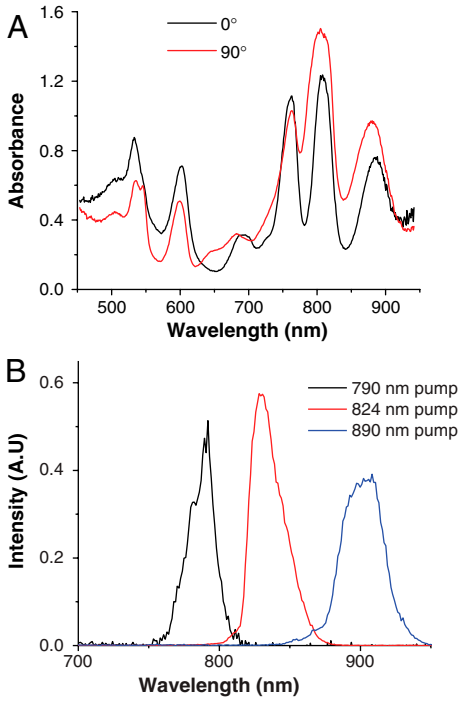

Fig. S1. Part (*A*) shows polarized ground state optical absorption for a typical single *R. sphaeroides* wild-type (WT) RC crystal ($P2_12_12_1$) at 100 K. The ground state absorption spectra are measured with light polarized perpendicular (90°) and parallel (0°) to the long axis of the crystal. (*B*) Pump spectra for the three pump wavelengths employed for the data shown in Figs. 2, 3; Figs. S2, S3, S4, and S5.

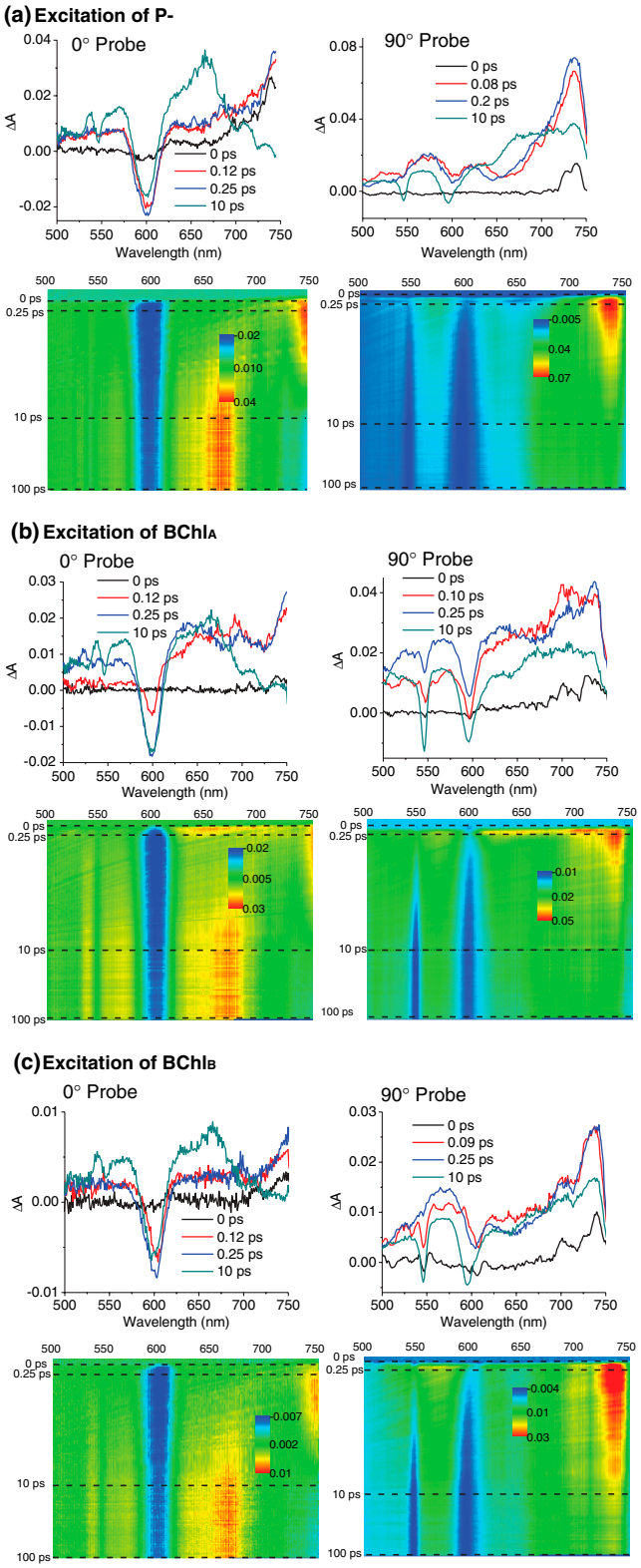

Fig. S2. Pump wavelength-dependent patterns of transient optical absorption changes for 0° and 90° probe in a single *Rb. sphaeroides* -wt crystal. The pump is adjusted to 890 nm (90°), 820 nm (0°), 790 nm (90°), in parts (*A*, *B*, and *C*), to selectively pump Q_y optical transitions of P_-, $BChl_A$, and $BChl_B$, respectively. The crystal temperature is 100 K. The bottom graphs are 2D graphs that illustrate the time-progression of the transient absorption spectra. Data are taken from the same crystal as shown in Fig. 2 and Fig. 4.

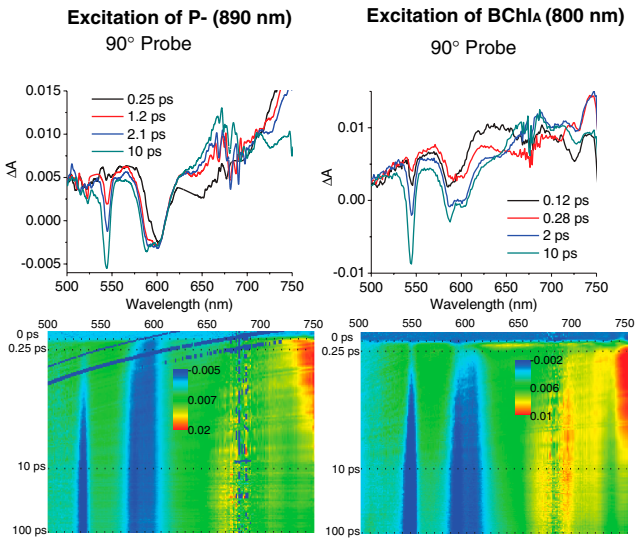

Fig. S3. Pump wavelength-dependent patterns of transient optical absorption changes for 90° probe in another single *Rb. sphaeroides*-wt crystal. The pump is adjusted to 890 nm (90°), and 800 nm (90°), as labeled. The crystal temperature is 100 K. The bottom graphs are 2D graphs that illustrate the time-progression of the transient absorption spectra. The horizontally streaks in the 2D pattern shown are the right resulted from nitrogen bubbles in the dewar.

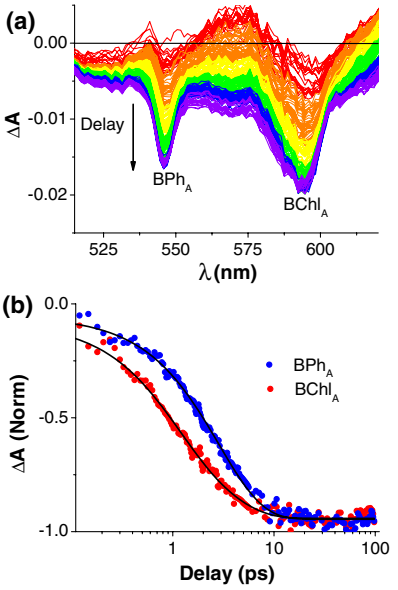

Fig. S4. Difference transient absorption spectra following formation of P*. The left box shows difference transient spectra recorded with delays from 150 fs to 80 ps, and following subtraction of the spectrum recorded with a 120 fs delay from the pump pulse. This subtraction removes contributions of ground state bleaching of P and highlights the time-progression of the BPh and BChl Q_X transient components. The right box shows single wavelength BPh_A and $BChl_A$ Q_X transient kinetics measured at 545 nm and 590 nm, respectively. The BPh_A 545 nm kinetics lag 0.9 ps behind the $BChl_A$ 590 nm kinetics. Excitation was provided by 890 nm pump pulse, and both pump and probe with 90° polarized, using the transient spectra shown in Fig. 2 and Fig. S2.

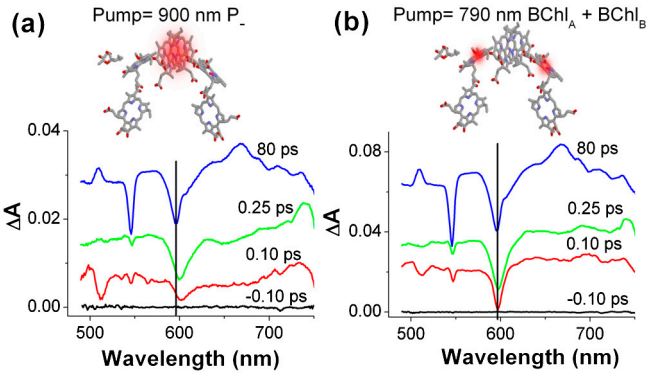

Fig. S5. Pump wavelength-dependent patterns of transient absorption detergent-solubilized *Rb. sphaeroides* -wt in solution at 100 K. The pump beam was depolarized and adjusted to 890 nm and 790 nm, in parts *A*, and *B*, respectively. Spectra are offset for clarity. The vertical line is placed at 595 nm in each box.

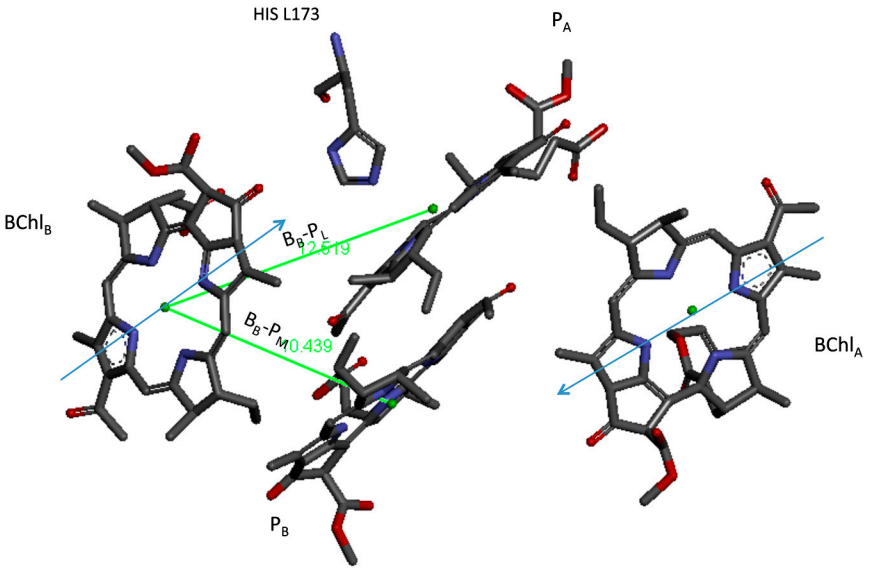

Fig. S6. The projection of possible charge-transfer (CT) transitions on the RC coordination.

Table S1. Cofactor Alignments with possible CT directionsΘ (cosΘ)

Possible CT pair	BPh_B	BPh_A	$BChl_A$
		Cofactor Qy	
$BChl_B$ Q_y	86.1° (0.07)	42.6° (0.74)	73.6° (0.28)
$BChl_B$-P_A	76.1° (0.24)	85.7° (0.07)	36.7° (0.80)
$BChl_B$-P_B	85.2° (0.08)	68.8° (0.36)	62.7° (0.46)
		Cofactor Qx	
$BChl_B$ Q_y	44.7° (0.71)	56.9° (0.54)	51.3° (0.62)
$BChl_B$-P_A	37.8° (0.79)	46.0° (0.69)	86.6° (0.06)
$BChl_B$-P_B	5.2° (0.99)	22.8° (0.92)	59.6° (0.51)